applied sciences

MDPI

Article

Anchorage Strength Model for Large-Diameter Headed Bars Anchored at the Cutoff Point

Hyung-Suk Jung

Department of Fire and Safety Engineering, Kyungnam University, 7 Gyeongnamdaehak-ro, Masanhappo-gu, Changwon-si 51767, Gyeongsangnam-do, Republic of Korea; junghs@kyungnam.ac.kr

Abstract

Design guidance for headed-bar development remains uncertain for large-diameter bars at cutoff points, where bar termination increases anchorage demand and confinement is often limited. This study quantified the anchorage behavior of 43 and 57 mm headed bars and established a regression-based strength model grounded in a splitting-controlled bond–bearing mechanism. Nineteen reinforced concrete beam specimens were tested under four-point loading configured to place the bending-moment inflection point at the head location. The primary variables were the development length (l_{dt} = 12–28d_b), concrete compressive strength ($f_c{}'$ = 42 and 70 MPa), clear side cover, clear spacing, and transverse reinforcement index (K_{tr}/d_b = 0–2.0). All the specimens failed by splitting prior to bar yielding, characterized by longitudinal cracking along the development region and cover spalling near the head. The anchorage strength increased with concrete compressive strength and development length and was most strongly enhanced by transverse reinforcement (up to ~60%). At failure, the bond contributed 70–86% of the developed stress, while the head-bearing contribution increased with confinement. Existing ACI 318-19 and KDS-2021 provisions were generally unconservative, particularly for unconfined specimens. The proposed bond–bearing model showed a close agreement with the test database (mean test/prediction = 0.99; COV = 4.72%) within stated parameter limits.

Keywords: large-diameter headed bars; anchorage strength; cutoff region

1. Introduction

The anchorage performance of reinforcing bars is critical in improving the strength and ductility of reinforced concrete (RC) members [1,2]. When geometric constraints or reinforcement congestion preclude the provision of sufficient development length for straight bars, standard hooks or headed bars are commonly employed as alternatives [3–5]. With the increasing trend toward high-rise and large-scale structures, the use of large-diameter reinforcing bars has become increasingly prevalent. Owing to their increased bar diameters, current design codes generally require longer development lengths for large-diameter bars [6,7]. Specifically, in congested regions, such as beam–column joints, providing a sufficient development length for large-diameter reinforcement is often challenging, and the resulting constructability challenges and bar interference can become major factors limiting the structural performance. Accordingly, as the application of large-diameter and high-strength reinforcements expands, the demand for achieving equivalent performance with shorter development lengths has increased. In this context, large-diameter headed bars have attracted significant attention as practical alternatives for securing the anchorage performance while reducing reinforcement congestion [8].

Check for updates

Received: 5 February 2026
Revised: 5 March 2026
Accepted: 6 March 2026
Published: 9 March 2026

Copyright: © 2026 by the author. Licensee MDPI, Basel, Switzerland. This article is an open access article distributed under the terms and conditions of the Creative Commons Attribution (CC BY) license.

Development length provisions for headed bars were first introduced in ACI 318-08 based on a study by Thompson et al. [9]. Subsequently, the provisions were revised in ACI 318-19 via additional experimental investigations, including those by Shao et al. [10–12]. As the development length equation was updated, the basic development length coefficient was modified to 1/31. In addition to the epoxy coating factor, modification factors accounting for the transverse reinforcement, bar location, and concrete strength were incorporated. Furthermore, the dependence of the development length on the bar diameter changed from a linear relationship to proportionality to the 1.5th power of the bar diameter [6]. Additionally, the maximum specified yield strength increased to 690 MPa, and the minimum clearance spacing requirement was reduced from 4 to $3d_b$ [6]. However, the applicable bar diameter is limited to 35 mm or less, which restricts the use of large-diameter headed bars with diameters exceeding 43 mm. This limitation is primarily attributed to a lack of experimental data on large-diameter headed bars [11,13]. Moreover, for large-diameter reinforcing bars, potential alterations in failure modes and anchorage resistance mechanisms may arise, thereby rendering a direct extrapolation of existing code provisions to larger bar sizes increasingly uncertain and potentially inappropriate [8].

Experimental and numerical studies have investigated the influence of reinforcing bar diameter on anchorage behavior [14–18]. In general, anchorage performance tends to deteriorate as the bar diameter increases. This tendency can be rationalized in terms of the inherent geometric scaling incompatibility between the tensile force to be developed in the bar and the interfacial area available for anchorage stress transfer. Specifically, the tensile force demand scales with the cross-sectional area of the bar, i.e., proportionally to the square of its diameter, whereas the interfacial area governing anchorage stress transfer increases only linearly with the diameter. Consequently, the average anchorage stress required to mobilize a given level of bar stress increases with bar diameter from a purely geometric standpoint. In addition, the radial pressure generated by rib bearing tends to increase with increasing bar diameter, assuming comparable relative rib geometry and stress levels, thereby inducing greater circumferential tensile stresses in the surrounding concrete. Within the framework of thick-walled cylinder mechanics, this enhanced radial pressure translates into amplified tensile stresses, which accelerate the initiation and propagation of splitting cracks. As a result, larger-diameter bars require higher average anchorage stresses to develop the same bar stress, which consequently leads to a reduction in nominal anchorage strength and increased susceptibility to anchorage-related splitting failure. However, some studies have reported that when sufficient concrete cover is provided, when a high transverse reinforcement index ensures effective confinement, or when high tensile-strength materials such as UHPC are employed, the influence of bar diameter on anchorage strength may diminish or, conversely, anchorage capacity may increase with increasing bar diameter [19,20]. This suggests that the diameter effect is not intrinsic but is strongly modulated by the level of confinement and the tensile resistance of the surrounding matrix.

Thompson et al. [5,21–23] conducted compression–compression–tension (CCT) node tests and lap-splice tests to investigate the anchorage behavior of headed bars with diameters of 25 and 36 mm; they systematically described the anchorage resistance mechanism and found that the anchorage resistance of the headed bars was provided by the combined contribution of the bond and head-bearings. The bond resistance governed the initial response, whereas, with an increasing load, the bond component reached its maximum and then began to decrease. During this process, the anchorage resistance was gradually transferred to the head-bearing component. At failure, the anchorage strength was governed by a combination of reduced bond resistance and increased bearing resistance. Similar behavior was observed under the CCT node and lap-splice conditions. Based on these observations, Thompson et al. proposed a predictive model that separates the bearing and bond components to estimate the anchorage strength.

Chun et al. [24] conducted lap-splice tests using high-strength headed bars with a diameter of 29 mm to investigate the anchorage behavior and evaluate the limitations of current design provisions. Bar spacing, side cover, and the presence of transverse reinforcement were considered as key variables, with particular emphasis on parameters not explicitly addressed in the headed-bar provisions of ACI 318. The test results showed that all the specimens exhibited splitting failure accompanied by cover spalling and that the prying action was significant in unconfined specimens. In contrast, the use of transverse reinforcement effectively restrained crack propagation and increased the anchorage strength, particularly for the head-bearing component. The study further indicated that the current provisions may be unconservative for unconfined lap splices of high-strength headed bars and proposed a regression-based prediction model for anchorage strength under lap-splice conditions.

Chun et al. [8,13,25,26] experimentally evaluated the anchorage performance of large-diameter headed bars (43 and 57 mm) in exterior beam–column joints and focused on the conditions governed by side-face blowout failure. They examined the effects of key variables, such as the development length, side cover, concrete compressive strength, and transverse reinforcement, on the developed bar stresses. Specifically, they reported that hairpin-type transverse reinforcement effectively delayed side-face blowout by restraining crack propagation, thereby increasing the anchorage strength. Furthermore, existing predictive models may either overestimate or underestimate the anchorage strength owing to differences in joint conditions and failure modes. Hence, a regression-based anchorage strength equation, accounting for side-face blowout failure, was proposed.

These previous studies indicate that the anchorage strength of headed bars cannot be readily generalized using a single design equation and that an approach that considers failure modes and anchorage conditions is required. The failure behavior of headed bars varies depending on the anchorage region, and the anchorage performance is strongly influenced by anchorage conditions such as the confinement provided by the transverse reinforcement. Therefore, for the practical application of large-diameter headed bars, design models that reflect the differences between the anchorage regions (e.g., joints, lap splices, and bar termination regions) must be established. This requires a systematic evaluation of the various parameters influencing the anchorage performance.

In RC structural design, the reinforcement is not always placed continuously along the entire member length; instead, the bars are often terminated (cutoff) at specific locations based on the required tensile force to realize an efficient design [27]. Such a cutoff point constitutes discontinuity zones where bar stresses change abruptly and the anchorage demand becomes concentrated [28]. Reinforcement congestion, limited available development lengths, and localized crack concentrations may occur simultaneously in these regions. Accordingly, headed bars, which can reduce the required development length, may provide an effective alternative at the cutoff point. Specifically, the efficient anchorage of large-diameter headed bars at the cutoff point has the potential to improve structural safety and constructability. Therefore, the anchorage behavior of large-diameter headed bars anchored at the cutoff point must be quantitatively verified, and the effects of anchorage conditions and the applicability of existing prediction models must be systematically evaluated. Additionally, given that the cutoff point involves constrained anchorage conditions and discontinuous stress transfer, the development of bonds and bearing resistance may differ. Hence, the anchorage mechanism and governing failure mode should be carefully examined.

In this study, the anchorage behavior of large-diameter headed bars anchored at the cutoff point was systematically evaluated, and the effects of key variables, including cover, spacing, concrete strength, and confinement provided by the transverse reinforcement, as well as the influence of governing failure modes, were quantified. Furthermore, an experimental design model was proposed by incorporating the bond–bearing resistance mechanism and the dependence on failure mode, thereby providing a rational basis for addressing the limitations of current design provisions for high-strength and large-diameter headed bars, including the effects of transverse reinforcement and failure modes.

2. Experimental Program

2.1. Specimen Variables

Figure 1 shows the representative specimen configuration for simulating the cutoff point. Two headed bars serving as longitudinal reinforcements for the beam were embedded within the cutoff point. All the specimens were designed to fail by splitting prior to the yielding of the headed bars. Based on existing studies, the primary variables affecting the anchorage strength of headed bars are the following: bar diameter (d_b), concrete compressive strength (f_c'), development length (l_{dt}), clear side cover (c_{so}), clear spacing between the headed bars (c_{si}), and transverse reinforcement index (K_{tr}) [8,9,12,21,22,24,29,30]. To investigate the anchorage performance of large-diameter headed bars beyond the applicability range of ACI 318-19, some variables were selected considering the minimum code requirements and practical field applications. In this study, the cutoff point was defined as the development region of the headed bars corresponding to the development length.

Two headed bars 43 and 57 mm in diameter were deliberately selected to exceed the applicability limits of the current ACI 318-19 [6] provisions for headed-bar development. By adopting bar sizes outside the code range, we ensured that the test program directly evaluated anchorage behavior in regions where existing design equations are not supported by experimental data. Two target concrete compressive strengths, 42 and 70 MPa, were selected to represent normal- and high-strength concrete commonly used in modern RC construction. Table 1 presents a summary of the measured compressive strengths on the test day, determined in accordance with ASTM C39/C39M [31].

The development length of the headed bars varied from $12d_b$ to $28d_b$. This range was intentionally selected so that splitting failure would govern within the development zone over a wide spectrum of embedment lengths, thereby enabling an observation of the progressive mobilization of the bond and head-bearing actions as a function of the development length. Accordingly, five discrete development lengths—$12d_b$, $15d_b$, $18d_b$, $23d_b$, and $28d_b$—were adopted. To evaluate the influence of the surrounding concrete on splitting resistance, two parameters were considered: the clear side cover (c_{so}) and the clear spacing between the headed bars (c_{si}). Current design provisions regard these dimensions as indicators of the effective concrete thickness resisting splitting [8,11,24]. Accordingly, the test matrix was configured to vary both parameters independently to quantify their individual and combined effects under cutoff anchorage conditions. Two side cover values, $2d_b$ and $3d_b$, were adopted, both satisfying or exceeding the minimum code requirement. Three clear spacings—$4d_b$, $3d_b$, and $2d_b$—were selected. The $4d_b$ and $3d_b$ cases conform to the requirements of ACI 318-19 [6], whereas the $2d_b$ case represents a realistic yet highly congested detailing condition frequently encountered with large-diameter reinforcements. Two categories of specimens were prepared to investigate the role of transverse confinement. Unconfined specimens were constructed without transverse reinforcement within the development zone, as shown in Figure 1a, so that splitting resistance was provided solely by the surrounding concrete. In contrast, confined specimens incorporated uniformly spaced closed stirrups throughout the development zone, as shown in Figure 1b, to provide confinement against crack propagation. The level of transverse confinement was quantified using the transverse reinforcement index (K_{tr}), calculated in accordance with the provisions of ACI 318-19 [6]. Two confinement levels, corresponding to K_{tr}/d_b ratios of 1.0 and 2.0, were examined.

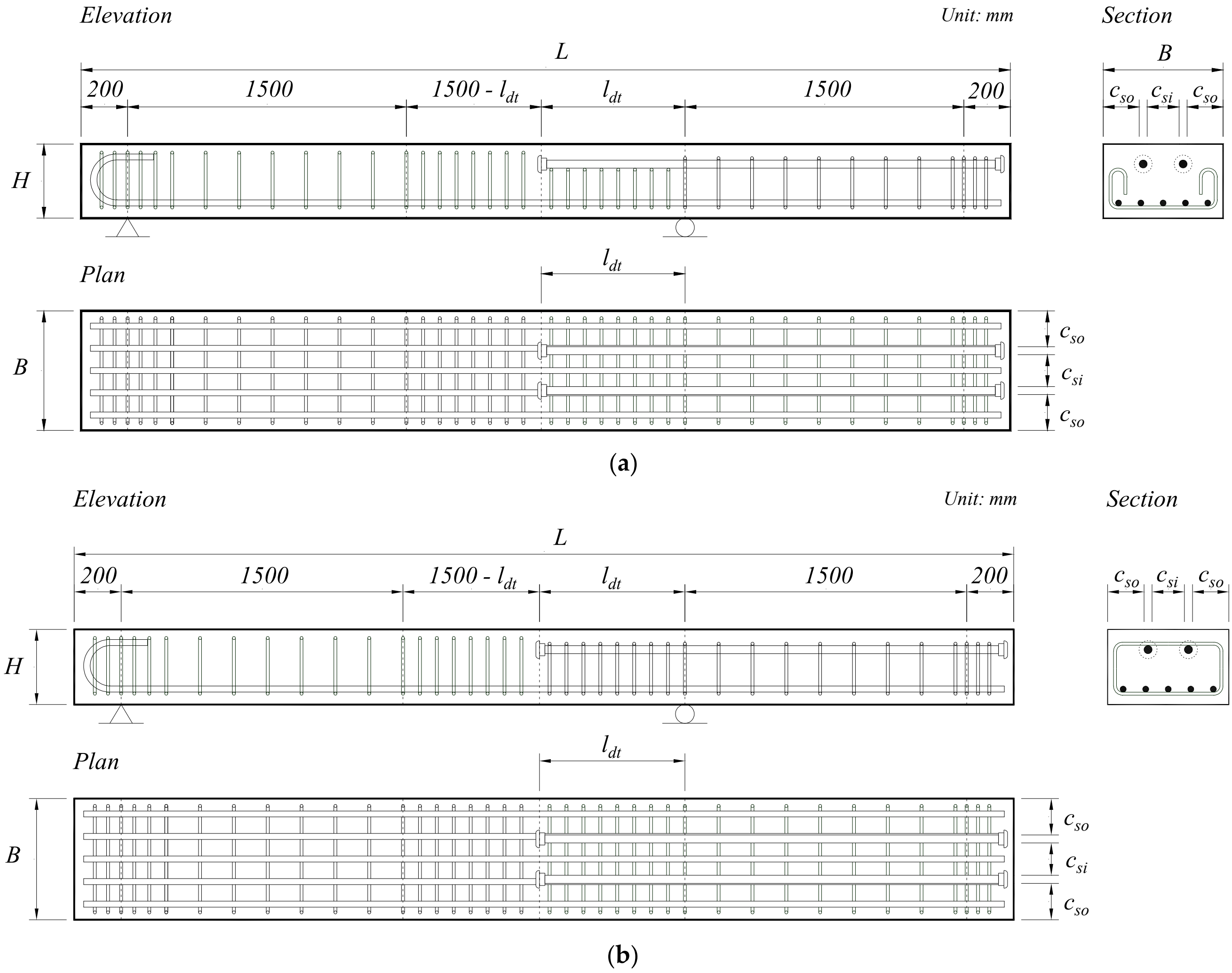

Figure 1. Details of test specimens: (**a**) unconfined specimens; (**b**) confined specimens.

Table 1. Details of test specimens.

Specimen *	d_b [mm]	f'_c [MPa]	l_{dt}/d_b	c_{si}/d_b	c_{so}/d_b	K_{tr}/d_b	B [mm]	H [mm]	L [mm]
#14-F42-L12-S4-C2	43	48.3	12	4.0	2.0	-	430	400	3500
#14-F42-L15-S3-C2	43	48.3	15	3.0	2.0	-	387	400	3500
#14-F42-L15-S2-C2	43	48.3	15	2.0	2.0	-	344	400	3500
#14-F42-L18-S4-C3	43	46.7	18	4.0	3.0	-	516	400	4900
#14-F42-L23-S4-C2	43	46.7	23	4.0	3.0	-	516	400	4900
#14-F42-L28-S4-C2	43	46.7	28	4.0	3.0	-	516	400	4900
#18-F42-L12-S4-C2	57	48.3	12	4.0	2.0	-	570	570	4500
#18-F42-L15-S3-C2	57	48.3	15	3.0	2.0	-	513	570	4500
#18-F42-L15-S2-C2	57	48.3	15	2.0	2.0	-	456	570	4500
#14-F70-L12-S4-C2	43	74.2	12	4.0	2.0	-	430	400	3500
#14-F70-L18-S4-C3	43	75.8	18	4.0	3.0	-	516	400	4900

Table 1. *Cont.*

Specimen *	d_b [mm]	f'_c [MPa]	l_{dt}/d_b	c_{si}/d_b	c_{so}/d_b	K_{tr}/d_b	B [mm]	H [mm]	L [mm]
#18-F70-L12-S4-C2	57	74.2	12	4.0	2.0	-	570	570	4500
#14-F42-L15-S2-C2-T1	43	48.3	15	2.0	2.0	1.0	344	400	3500
#14-F42-L18-S4-C3-T1	43	46.7	18	4.0	3.0	1.0	516	400	4900
#14-F42-L23-S4-C2-T1	43	46.7	23	4.0	3.0	1.0	516	400	4900
#18-F42-L15-S2-C2-T1	57	48.3	15	2.0	2.0	1.0	456	570	4500
#14-F42-L15-S2-C2-T2	43	48.3	15	2.0	2.0	2.0	344	400	3500
#14-F42-L18-S4-C3-T2	43	46.7	18	4.0	3.0	2.0	516	400	4900
#18-F42-L15-S2-C2-T2	57	48.3	15	2.0	2.0	2.0	456	570	4500

* #①-F②-L③-S④-C⑤-T⑥: ① is bar diameter (d_b); ② is design compressive strength of concrete; ③ is development length (l_{dt}/d_b); ④ is clear spacing between headed bars (c_{si}/d_b); ⑤ is side cover (c_{so}/d_b); ⑥ is transverse reinforcement index (K_{tr}/d_b); B is the width of specimen section; H is the height of the specimen section; L is the specimen length.

In total, 19 specimens were fabricated and tested: 13 with 43 mm headed bars and 6 with 57 mm headed bars. The combination of variables was configured to systematically examine the interaction between the development length, surrounding concrete thickness, and transverse confinement under cutoff anchorage conditions. Table 1 presents a detailed configuration of each specimen.

2.2. Materials, Test Setup and Instrumentation

The specified yield strength of the headed bars was 550 MPa for all the specimens. The measured yield strength (f_y) and tensile strengths (f_u) were 619 and 754 MPa for the 43 mm bars and 557 and 748 MPa for the 57 mm bars, respectively (Figure 2). Table 2 presents the main geometric details of the headed bars. The circular heads of the headed bars were used such that the net bearing area of the head (A_{brg}) exceeded four times the bar cross-sectional area (A_b), in accordance with the requirements of ACI 318-19 [6].

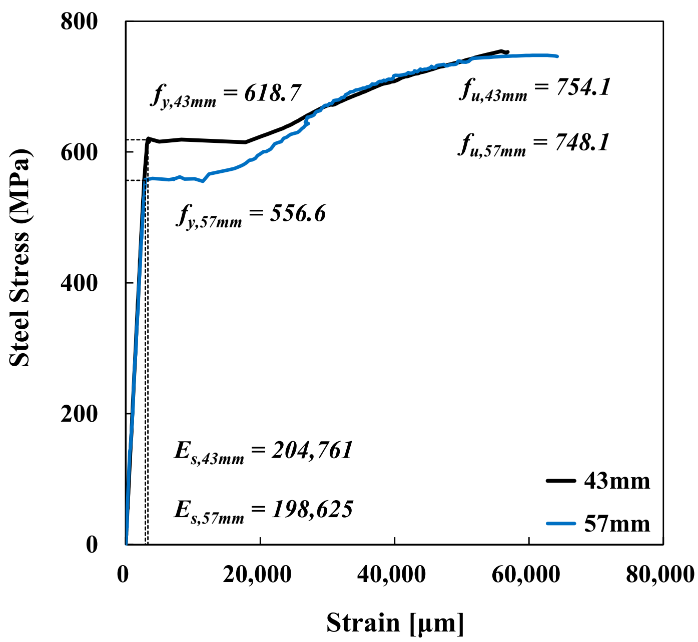

Figure 2. Stress–strain relationship of reinforcing bars obtained from uniaxial tensile tests.

Table 2. Head dimensions.

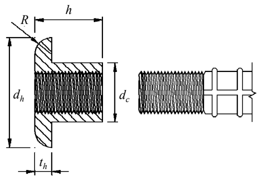

Headed Bar Diameter [mm]	d_h [mm]	t_h [mm]	R [mm]	h [mm]	d_c [mm]
43	96	19	22	48	65
57	128	25	26	63	85

The concrete mixtures were proportioned to achieve target 28-day compressive strengths of 42 MPa and 70 MPa. The water-to-cement ratios were set at 0.50 and 0.26, respectively. Ordinary Portland Cement was used in all specimens. Crushed granite coarse aggregate with a nominal maximum size of 20 mm and natural river sand were employed as the coarse and fine aggregates, respectively. The mix proportions were determined in accordance with established concrete mix design procedures to ensure adequate workability and consistent strength development. A summary of the detailed mixture proportions is provided in Table 3. All headed bar specimens were tested at a concrete age of 28 days. The compressive strengths reported in Table 1 correspond to the measured 28-day compressive strengths obtained on the date of testing. Therefore, the material properties adopted in the subsequent analyses of the experimental results are based on the measured 28-day compressive strengths, thereby ensuring uniformity and comparability among all specimens.

Table 3. Mix proportions of concrete.

Design Strength [MPa]	Water-to-Cement Ratio	Max Agg. Size [mm]	Unit Weight [kg/m^3]					
			Water	Cement	Fine Agg.	Coarse Agg.	Fly Ash	Admixture
42	0.50	20	165	330	765	955	83	3.8
70	0.26	20	165	630	628	842	70	7.0

As shown in Figure 3a, the loading configuration was designed to reproduce the stress state of the headed bars anchored at a cutoff location. Two actuators, each with a capacity of 2000 kN, were used to apply the load. All specimens were tested under monotonic load-controlled conditions using a servo-controlled actuator. The loading rate was maintained at a constant rate of 12.5 kN/min. Loading was applied continuously without any intermediate unloading or hold intervals. Data were recorded at a sampling frequency of 1 Hz. The test was terminated when the applied load decreased by more than 20% from the maximum load, which was taken to indicate post-peak instability and loss of load-carrying capacity. The load was applied while maintaining a constant load ratio between the actuators such that the inflection points of the bending moment diagram coincided with the head location of the headed bars, thereby simulating a cutoff condition. This arrangement ensured that the development zone was subjected to combined bending and shear stresses representative of cutoff anchorage conditions. The specimens were proportioned to ensure flexural behavior without shear failure prior to splitting failure.

The instrumentation program measured the load–deflection response and headed bar strains. Two strain gauges were installed at two locations on each headed bar. One strain gauge was mounted on the head surface to measure the bearing stress developed by the head. The other strain gauge was installed at the end of the development region, where the maximum moment was applied, to measure the anchorage stress of the headed bar. Figure 3b shows the measurement locations.

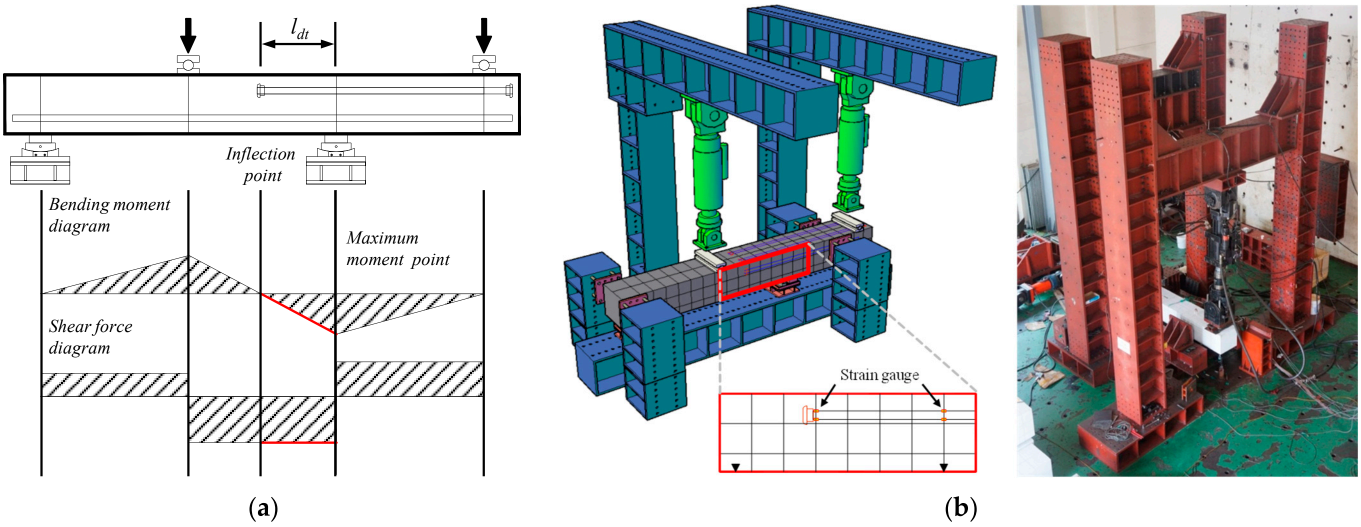

Figure 3. Details of the test specimen and test set-up: (**a**) test method concept; (**b**) experimental set-up.

3. Experimental Results and Discussion

3.1. Overall Behavior and Failure Modes

At the early stage of loading, flexural cracks were observed in the region of maximum bending moment near the end of the development zone. With increasing applied load, the cracks gradually propagated toward the headed end, indicating progressive stress transfer along the development zone with increasing bending moment. Following these flexural cracks, longitudinal cracks formed parallel to the headed bars, indicating the onset of splitting in the surrounding concrete.

In the unconfined specimens, splitting cracks within the development zone became increasingly pronounced with increasing load. Crack localization was particularly evident near the head region, where sudden spalling of the concrete cover above the head eventually occurred, as shown in Figure 4a. As shown in Figure 5, this resulted in a brittle loss of load-carrying capacity, as the concrete cover detached abruptly once the splitting cracks reached a critical width. The cracking pattern indicated that the surrounding concrete could no longer sustain the tensile stresses induced by the combined action of stress transfer along the bar and localized compression beneath the head.

In contrast, the confined specimens exhibited a distinctly different crack development. Although longitudinal splitting cracks were also formed, their growth was significantly restrained by the presence of transverse reinforcement. Rather than propagating freely along the development length, these cracks interacted with multiple transverse flexural cracks, forming a distributed cracking pattern across the specimen depth, as shown in Figure 4b,c. With increasing load, the cracks gradually widened and interconnected, resulting in greater deformation capacity compared with the unconfined specimens (Figure 5).

The difference in behavior between the two specimen groups can be attributed to the restraining role of the transverse reinforcement. In the absence of confinement, crack propagation was governed primarily by the limited tensile capacity of the concrete within the development region, leading to rapid crack extension toward the head and sudden spalling of the upper concrete cover. In contrast, when transverse reinforcement was present, the development of splitting cracks was partially restrained, promoting crack propagation across the specimen depth rather than directly along the headed bar.

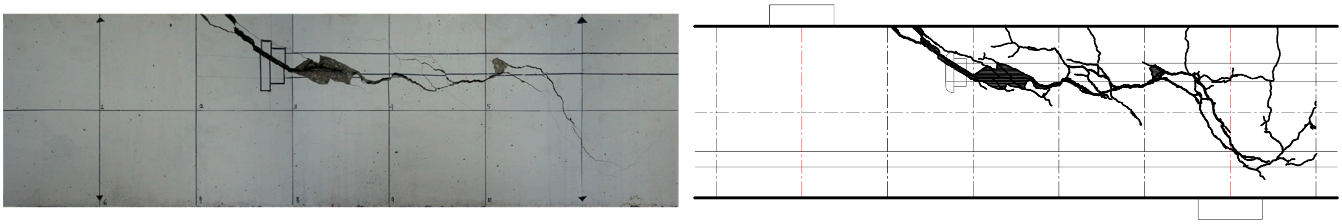

(**a**)

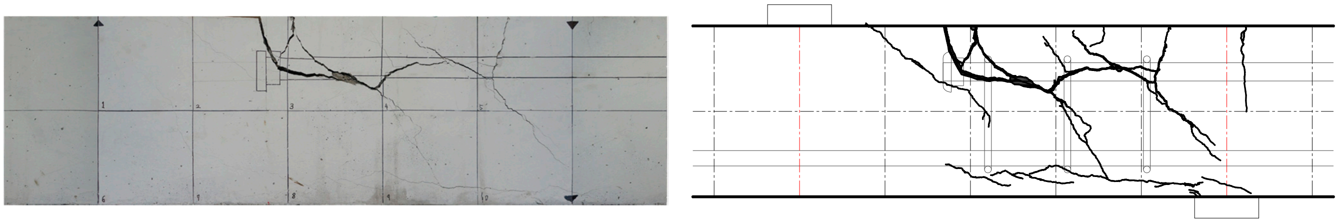

(**b**)

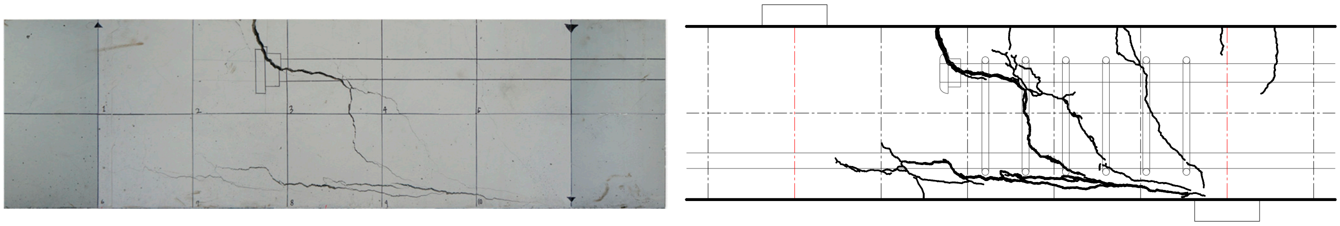

(**c**)

Figure 4. Crack patterns and failure modes of specimens: (**a**) unconfined specimen; (**b**) confined specimen (K_{tr}/d_b = 1.0); (**c**) confined specimen (K_{tr}/d_b = 2.0). The reference grid corresponds to a 200 mm × 200 mm square mesh. The maximum crack opening widths measured at peak load were approximately 15.7 mm, 11.6 mm, and 8.8 mm for specimens (**a**), (**b**), and (**c**), respectively.

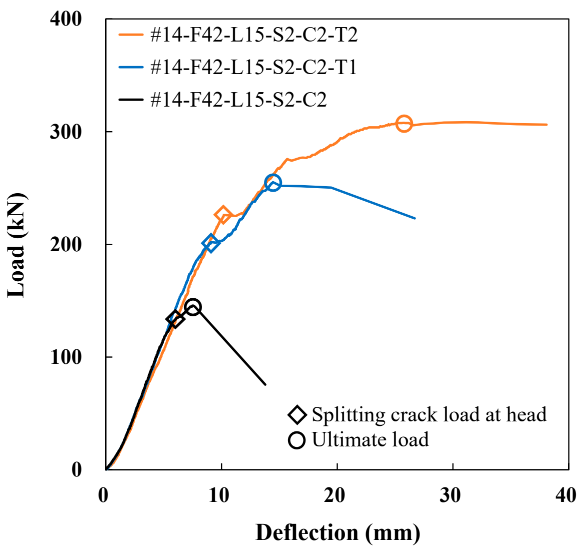

Figure 5. Load–deflection curves of unconfined and confined specimens.

Irrespective of the confinement condition, the final failure of all the specimens was governed by the splitting failure of the surrounding concrete rather than yielding of the headed bars. As intended, splitting cracks developed along the development length of the headed bars, as shown in Figure 6, and the final failure was characterized by spalling of the upper concrete cover in the head region. This splitting failure can be attributed to the combined effect of wedging forces induced by head bearing and prying action associated with flexural deformation, as illustrated in Figure 6. The failure behavior is consistent with the failure mechanisms reported in previous lap-splice experimental studies [5,24]. Particularly in the confined specimens, the transverse reinforcement effectively restrained this failure behavior.

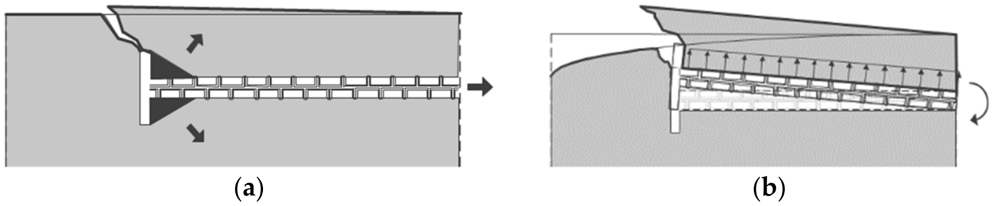

Figure 6. Failure mechanism: (**a**) wedging forces induced by head bearing; (**b**) prying action associated with flexural deformation.

3.2. Anchorage Strength of Headed Bars

The anchorage strength of each specimen was determined from the strain measured by a gauge installed near the end of the development zone, corresponding to the region of maximum bending moment. The measured strain was subsequently converted into the corresponding bar stress using the experimentally obtained stress–strain relationship of the reinforcing steel derived from uniaxial tensile tests (see Figure 2). The measured peak load was additionally converted into the corresponding bar stress through a sectional moment–curvature analysis to verify this estimation. In the sectional moment–curvature analysis, the uniaxial compressive stress–strain behavior of concrete was represented using the constitutive model proposed by Collins and Mitchell [32]. The tensile resistance of concrete was excluded from the analysis. The reinforcing steel was modeled using a bilinear elastic–perfectly plastic constitutive law, with strain hardening omitted for simplification. Using the measured material properties and cross-sectional geometry, we first determined the maximum bending moment at failure and then back-calculated the stress developed in the headed bars from this moment. The bar stress corresponding to this failure state was defined as the anchorage strength; Table 4 presents the results.

The anchorage strength varied based on the test variables as follows. A comparison between specimens with 43- and 57-mm bars showed that, on average, the anchorage strength of the 43 mm specimens was approximately 2.4% higher than that of the 57 mm specimens, indicating that the difference in the anchorage strength between the two diameters was small when the other variables were kept identical. This trend did not follow the implication of current design provisions [6,7]. Within the tested diameter range of 43 and 57 mm, the influence of bar diameter on the developed stress was found to be comparatively minor relative to other governing variables; therefore, bar diameter was not considered as an independent variable in the subsequent analytical formulations.

A comparison between specimens with design compressive strengths of 42 and 70 MPa showed that, on average, the anchorage strength of the 70 MPa specimens was approximately 23.1% higher than that of the 42 MPa specimens. This trend is consistent with current design provisions and previous experimental findings [6–8,11,21,24]. Specimens with longer development lengths consistently exhibited higher anchorage strengths. A comparison between specimens with development lengths of $18d_b$, $23d_b$, and $28d_b$ showed that the $28d_b$ specimens exhibited approximately 41.8% higher anchorage strength than the $18d_b$ specimens, whereas the $23d_b$ specimens showed an increase of approximately 22.7% relative to the $18d_b$ specimens, indicating that stress transfer occurred over a longer portion of the development zone prior to the onset of splitting failure. Examination of the effects of clear side cover and clear spacing showed that the clear side cover had no significant influence on the anchorage strength, whereas the clear spacing had a significant influence. A comparison between specimens with clear spacings of $3d_b$ and $2d_b$ indicated that, on average, the specimens with $3d_b$ spacing exhibited approximately 29.9% higher anchorage strength than those with $2d_b$ spacing.

Among the variables, the presence of transverse reinforcement had the most significant influence on the anchorage strength. On average, the confined specimens exhibited approximately 39.8% higher anchorage strength than the unconfined specimens. For specimens with transverse reinforcement indices of K_{tr}/d_b = 1.0 and 2.0, the anchorage strength increased by approximately 24.5% and 60.2%, respectively, compared with the unconfined condition, indicating that the confinement provided by transverse reinforcement restrained the widening of splitting cracks and allowed greater stresses to be sustained prior to failure.

Table 4. Comparison of experimental results with model predictions.

Specimen	f_{dt} [MPa]	$f_{dt,ACI}$ [MPa]	$f_{dt,KDS}$ [MPa]	f_{be} [MPa]	f_{be}/f_{dt}	$f_{be,Tho}$ [MPa]	$f_{be,ACI}$ [MPa]	f_{bo} [MPa]	f_{bo}/f_{dt}	$f_{bo,Ora}$ [MPa]	$f_{bo,ACI}$ [MPa]
#14-F42-L12-S4-C2	297	394	347	81	0.274	270	203	216	0.726	316	296
#14-F42-L15-S3-C2	341	489	431	67	0.198	230	178	274	0.802	313	306
#14-F42-L15-S2-C2	261	493	434	59	0.227	189	153	202	0.773	261	286
#14-F42-L18-S4-C3	414	493	434	87	0.210	366	300	327	0.790	573	533
#14-F42-L23-S4-C2	508	905	797	78	0.153	366	300	430	0.847	491	468
#14-F42-L28-S4-C2	587	743	655	83	0.141	366	300	504	0.859	409	402
#18-F42-L12-S4-C2	301	582	513	71	0.237	270	205	230	0.763	316	296
#18-F42-L15-S3-C2	337	741	653	58	0.174	230	179	279	0.826	313	306
#18-F42-L15-S2-C2	261	342	347	54	0.207	189	154	207	0.793	261	286
#14-F70-L12-S4-C2	363	424	431	104	0.286	189	153	259	0.714	366	358
#14-F70-L18-S4-C3	524	428	434	117	0.224	189	153	407	0.776	470	431
#18-F70-L12-S4-C2	363	428	434	94	0.258	366	300	269	0.742	648	578
#14-F42-L15-S2-C2-T1	369	493	434	109	0.295	366	300	260	0.705	532	488
#14-F42-L18-S4-C3-T1	493	493	434	149	0.302	366	300	344	0.698	655	574
#14-F42-L23-S4-C2-T1	536	743	655	151	0.282	189	154	385	0.718	366	358
#18-F42-L15-S2-C2-T1	345	582	513	101	0.293	189	154	244	0.707	470	431
#14-F42-L15-S2-C2-T2	458	582	513	117	0.255	270	203	341	0.745	316	296
#14-F42-L18-S4-C3-T2	548	428	434	163	0.297	230	178	385	0.703	313	306
#18-F42-L15-S2-C2-T2	451	428	434	122	0.271	189	153	329	0.729	261	286

Note: f_{dt} is the strength of headed bars obtained from the test; $f_{dt,ACI}$ is the strength of the headed bars predicted by the ACI 318 model; $f_{dt,KDS}$ is the strength of the headed bars predicted by the KDS-2021 model; f_{be} is the stress from head-bearing; $f_{be,Tho}$ is the stress from head-bearing predicted by the Thompson model; $f_{be,ACI}$ is the stress from head-bearing predicted by the ACI 318 model; f_{bo} is the stress from bond; $f_{bo,Ora}$ is the stress from bond predicted by the Orangun model; and $f_{bo,ACI}$ is the stress from bond predicted by the ACI 408 model.

The measured anchorage strengths were compared with the predictions of existing design models, including ACI 318-19 [6] and KDS 2021 [7]. As shown in Figure 7, both the models exhibited considerable scatter in the predictions and a consistent tendency toward unconservative results, particularly under unconfined conditions. The mean test-to-prediction ratios for the unconfined specimens were 0.719 and 0.777 using the ACI and KDS models, respectively. In contrast, for the confined specimens, the corresponding ratios improved to 0.864 and 0.941, indicating that the current design equations are more reliable when transverse reinforcement is present. These results suggest that existing design provisions do not fully capture the anchorage behavior of large-diameter headed bars under cutoff anchorage conditions, particularly when the confinement effect is limited. The experimental observations highlight the need for a model that can explicitly account for the effects of concrete compressive strength, development length, and transverse reinforcement index on the stress developed in headed bars at failure.

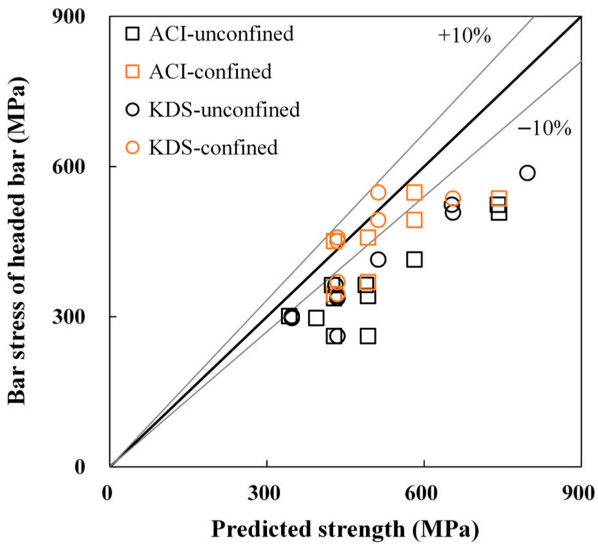

Figure 7. Comparison between measured bar stresses and predictions by ACI 318-19 and KDS-2021.

3.3. Contributions of Bond and Head Bearing to Bar Stress

Previous studies have shown that the anchorage strength of headed bars can be evaluated as the combined contribution of the bearing stress at the head and the bond stress along the deformed bar [3,9,10,12,21]. In this study, to examine how stresses were transferred within the headed bars, strain gauges installed on the head surface and at the critical section near the end of the development region were used to separate the contributions of these two stress-transfer mechanisms. The measured strains were converted into the corresponding stresses using the experimentally established stress–strain relationship of the reinforcing steel obtained from uniaxial tensile tests (see Figure 2). The strain recorded at the head was interpreted as the stress attributable to head bearing, and the bearing stress acting over the net head-bearing area was assumed to be uniformly distributed, while the strain measured at the end of the development region (corresponding to the maximum bending moment location) was converted into the anchorage stress of the headed bar. The stress developed by the bond was then obtained by subtracting the bearing stress from the anchorage stress. Table 4 presents the calculated values.

The evolution of these two stress components was evaluated using representative specimens with identical geometric parameters but different levels of transverse confinement (#14-F42-L18-S2-C3, #14-F42-L18-S2-C3-T1, and #14-F42-L18-S2-C3-T2). As shown in Figure 8, in all cases, the bond-related stress component increased rapidly during the early loading stages with increasing total bar stress. However, as failure approached, this component decreased, while the stress component associated with head-bearing continued to increase. This tendency became more pronounced with increasing transverse reinforcement index. This overall behavior differed from that observed for headed bars anchored at beam–column joints and was more consistent with the behavior reported for headed bars anchored in lap-splice regions [5,8,21,24].

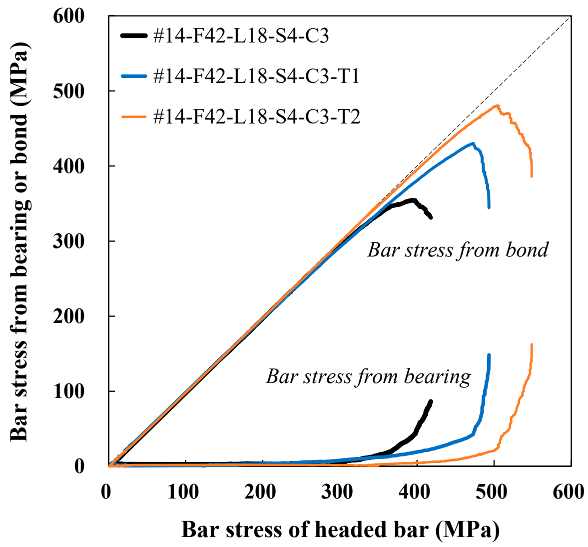

Figure 8. Bar stress from head bearing or bond in the anchorage.

At the failure state, the stress component attributed to the bond accounted for approximately 70% to 86% of the total developed bar stress, whereas the stress component associated with head bearing ranged from approximately 14% to 30%. The relative magnitude of these contributions varied primarily with the level of transverse confinement, with a noticeable increase in the head-bearing component with increasing confinement. These observations suggest that restraining the widening of splitting cracks induced by wedging forces and prying action allowed a greater portion of the stress to be mobilized through head bearing.

As shown in Figure 9a, the stress component attributed to head bearing was compared with predictions from existing analytical models. Both Thompson's model [24] and the provisions of ACI 318 [6] tended to overestimate the head-bearing stress for the unconfined specimens. The mean measured-to-predicted ratios for the unconfined specimens were 0.265 and 0.335 using the Thompson and ACI models, respectively, while the corresponding values for the confined specimens were 0.519 and 0.639. As shown in Figure 9b, the stress component attributed to the bond was compared with predictions from Orangun's model [33] and the recommendations of ACI 408R [34]. Unlike the trend observed for the head-bearing component, these models tended to overestimate the bond-related stress for the confined specimens. The mean measured-to-predicted ratios for the unconfined specimens were 0.806 and 0.820 using the Orangun and ACI 408R models, respectively, while the corresponding values for the confined specimens were 0.661 and 0.714. This trend is attributed to the interaction between the bearing and bond components. At the failure state, the bond-related stress decreased while the head-bearing stress increased, indicating that the reduction in the bond contribution was accompanied by an increase in the bearing contribution. Accordingly, with increasing transverse confinement, the head-bearing component increased while the bond component decreased.

These comparisons indicate that existing analytical models do not adequately represent the stress distribution developed in large-diameter headed bars under cutoff anchorage conditions. Accordingly, a dedicated anchorage strength model for large-diameter headed bars under cutoff conditions is required.

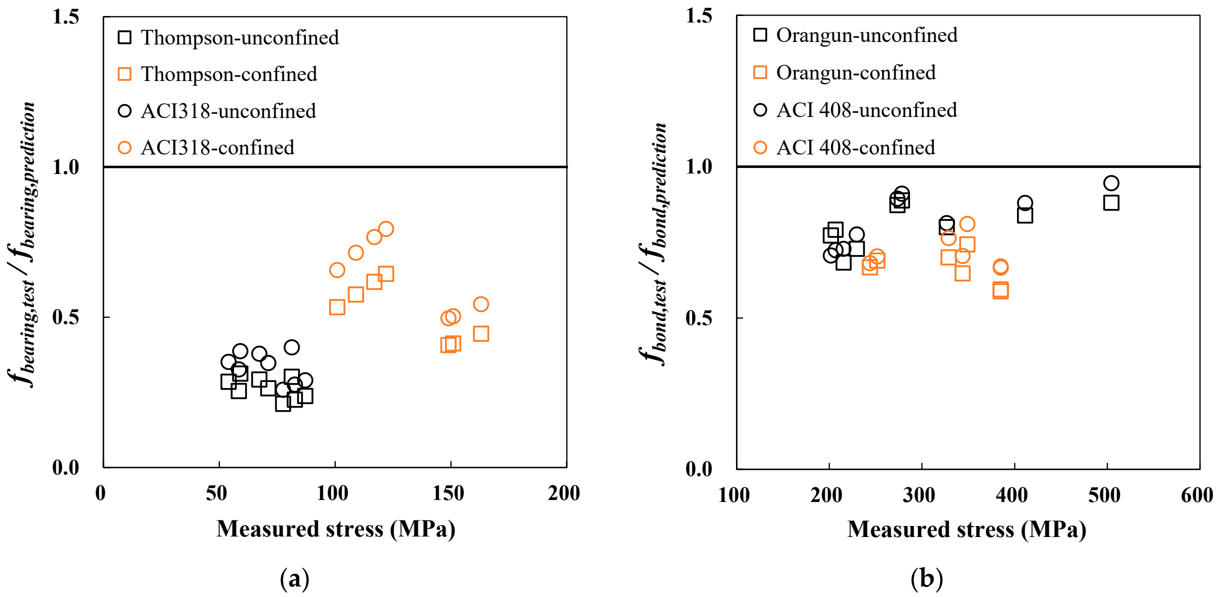

Figure 9. Comparison of experimental results with model predictions: (**a**) stress from head-bearing obtained using Thompson's and ACI318-19 models; (**b**) stress from bond obtained using Orangun and ACI 408 models.

4. Proposed Model for Anchorage Strength of Headed Bars

4.1. Effects of Concrete Compressive Strength

The influence of concrete compressive strength on the components constituting the anchorage strength of headed bars was first examined. For this purpose, specimens with identical test variables except for the concrete strength were selected, and their experimental results were directly compared. The measured concrete compressive strengths considered in this study were 46.7, 48.3, 74.2, and 75.8 MPa, as listed in Table 1. To evaluate how concrete strength affects each stress component, regression analyses were performed by assuming a power relationship of the form $(f_c')^{\alpha}$. Two comparison cases were established using specimens that differed only in terms of the concrete strength while maintaining identical development length, spacing, cover, and transverse reinforcement index. From these cases, the exponent α was determined separately for the head-bearing stress component and the bond stress component.

As shown in Figure 10, for the first comparison case (46.7 and 75.8 MPa), the exponent α was found to be 0.64 for the head-bearing stress component and 0.43 for the bond stress component. For the second comparison case (48.3 and 74.2 MPa), the corresponding α values were 0.57 and 0.37. Although slight differences were observed between the two cases, both indicated that the relationship between the concrete strength and the developed stresses could be reasonably represented by an exponent close to 0.5. This trend is consistent with existing splitting-strength models [6,8,21,24]. Accordingly, in the proposed models for the head-bearing stress component and the bond stress component of headed bars, the effect of concrete compressive strength was taken to be proportional to $(f_c')^{0.5}$.

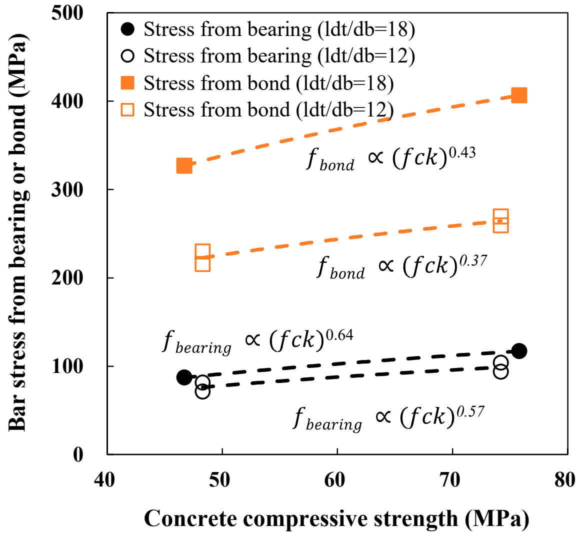

Figure 10. Correlation between concrete compressive strength and stresses from head-bearing or bond.

4.2. Effects of Development Length

The relationship between the development length and the head-bearing stress component and the bond stress component of headed bars was examined using unconfined specimens. To eliminate the influence of concrete strength, all the measured stresses were normalized by $(f_c')^{0.5}$ prior to comparison. This normalization enabled the influence of development length to be evaluated independently. Figure 11 shows the variation in the normalized head-bearing stress component and bond stress component with the development length expressed as l_{dt}/d_b. The normalized head-bearing stress component showed little variation within the investigated range of development lengths. The average normalized value of this stress was approximately 8.14 MPa, which was lower than the values reported in previous experimental studies on headed bars [23,24]. In contrast, the normalized bond stress component exhibited a clear increasing trend with increasing development length. A regression analysis of the normalized bond stress component with respect to l_{dt}/d_b produced a linear relationship. This trend is similar to that observed in existing development length design expressions for headed bars [6,7].

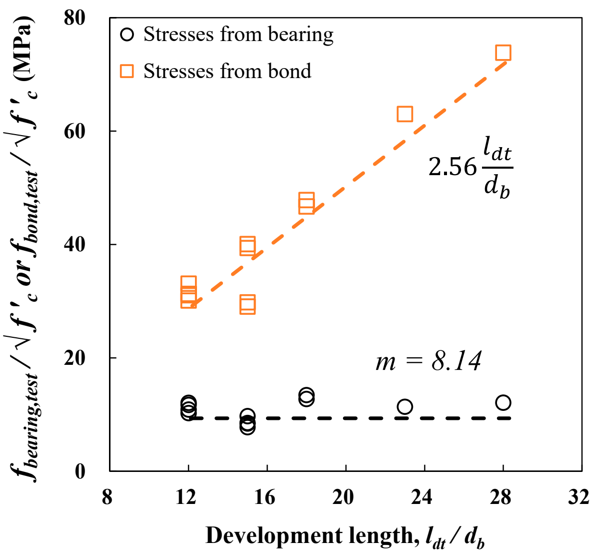

Figure 11. Correlation between development length and stresses from head bearing or bond.

Based on these analytical results, predictive expressions for the head-bearing stress component and the bond stress component were established for the unconfined specimens. From the average value of the normalized stress, the predictive expression for the head-bearing stress component of the unconfined specimens ($f_{hd,p,un}$) was derived as expressed in Equation (1).

$$f_{hd,p,un} = 8.14\sqrt{f'_c} \tag{1}$$

Furthermore, a regression analysis was performed to derive the predictive expression for the bond stress component of the unconfined specimens ($f_{bo,p,un}$), as presented in Equation (2).

$$f_{bo,p,un} = 2.56\frac{l_{dt}}{d_b}\sqrt{f'_c} \tag{2}$$

4.3. Effects of Clear Side Cover and Spacing Between the Headed Bars

Side cover and clear spacing between the headed bars are primary parameters influencing anchorage strength. In ACI 318-19, the side cover and one-half of the clear spacing are treated as equivalent parameters in evaluating the effective concrete thickness for development length [6]. Although this concept was originally formulated for straight-bar development, its extension to headed bars is supported by prior anchorage models, including the side-face blowout strength formulation for headed anchors [3,6] and the anchorage strength model for headed reinforcement lap splices [5,21], where splitting-controlled capacity is governed by the minimum available concrete confinement. In headed bars, wedging action and prying behavior occur, which induce tensile stresses in the surrounding concrete and initiate splitting cracks at the most vulnerable region. For specimens without transverse reinforcement, the anchorage resistance under splitting-controlled failure was assumed to be governed by the minimum effective concrete thickness. To quantify this effect, the effective concrete thickness (c_{min}) was defined as follows.

$$c_{min} = \min(c_{so},\ 0.5c_{si}) \tag{3}$$

where c_{so} is the clear side cover, and c_{si} is the clear spacing between headed bars.

Based on this theoretical assumption, the effects of side cover and clear spacing were integrated into a single parameter representing the effective concrete thickness susceptible to splitting failure. The effect of the effective concrete thickness was evaluated using only unconfined specimens in order to exclude the influence of transverse reinforcement and isolate the contribution of concrete confinement. As shown in Figure 12, specimens with smaller effective concrete thickness (c_{min} = 1.0) consistently exhibited lower head-bearing stresses and bond stresses, confirming that, under the present test conditions, the anchorage behavior of unconfined specimens is governed by the minimum effective concrete thickness.

Specimens with lower c_{min} values consistently exhibited lower head-bearing and bond stresses. To isolate the influence of c_{min} from the effects of concrete compressive strength and development length, the experimentally obtained head-bearing stress and bond stress were normalized by the predicted values from Equations (1) and (2), respectively. Figure 12 shows the relationship between the normalized stresses and the ratio c_{min}/d_b. With increasing c_{min}/d_b, both the normalized head-bearing stress and normalized bond stress increased, with a more pronounced increase observed in the head-bearing stress. This tendency can be attributed to the splitting behavior induced by wedging and prying actions near the head. When c_{min}/d_b is low, the surrounding concrete is less capable of resisting the wedging and prying actions generated in the vicinity of the head, resulting in premature splitting and reduced stress development. Because the influence of c_{min}/d_b

on the head-bearing stress and bond stress exhibited different trends, separate regression analyses were performed, resulting in the relationships expressed in Equations (4) and (5).

$$\varphi_{hb,un} = 0.484\frac{c_{min}}{d_b} + 0.473 \quad (4)$$

$$\varphi_{bo,un} = 0.224\frac{c_{min}}{d_b} + 0.594 \quad (5)$$

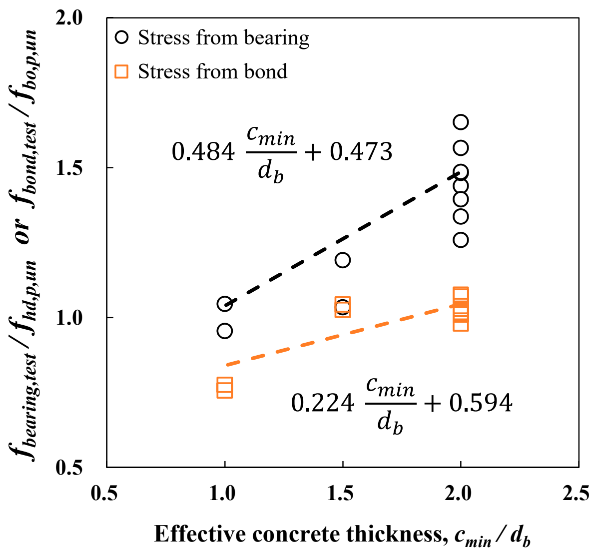

Figure 12. Correlation between effective concrete thickness and stresses from head bearing or bond.

4.4. Effects of Transverse Reinforcement

Among the test variables, the transverse reinforcement exhibited the most significant influence on both the head-bearing and bond stresses. Similar observations were reported in previous lap-splice tests, where transverse reinforcement was identified as the dominant variable affecting anchorage performance. Compared with the unconfined specimens, specimens with transverse reinforcement showed, on average, a 39.8% increase in stress. For specimens with K_{tr}/d_b = 1.0, the head-bearing stress increased by 73.3% and the bond stress by 14.2%, relative to the unconfined specimens. When K_{tr}/d_b = 2.0, the head-bearing stress increased by 103.6% and the bond stress by 48.6%.

This tendency is attributed to the role of transverse reinforcement in resisting splitting cracks that develop along the development region. By restraining the splitting induced by wedging and prying actions near the head, the transverse reinforcement delays splitting failure and allows greater stress development. With increasing transverse reinforcement index, this restraining effect becomes more effective. The enhancement is more pronounced in the head-bearing stress than in the bond stress.

To isolate the effect of transverse reinforcement and to directly quantify the increase in the stresses of confined specimens relative to the unconfined baseline, the experimentally obtained head-bearing stress and bond stress were normalized using the predicted values from Equations (1) and (2), respectively. Figure 13 shows the relationship between the normalized stresses and the ratio K_{tr}/d_b. This normalization allows the pure contribution of transverse reinforcement to be evaluated without the influence of effective concrete thickness. The effect of transverse reinforcement was incorporated into the effective concrete thickness term. Separate regression analyses of the confined specimens resulted in the relationships expressed in Equations (6) and (7):

$$\varphi_{hb} = \varphi_{hb,un} + 0.744\frac{K_{tr}}{d_b} \quad (6)$$

$$\varphi_{bo} = \varphi_{bo,un} + 0.145\frac{K_{tr}}{d_b} \quad (7)$$

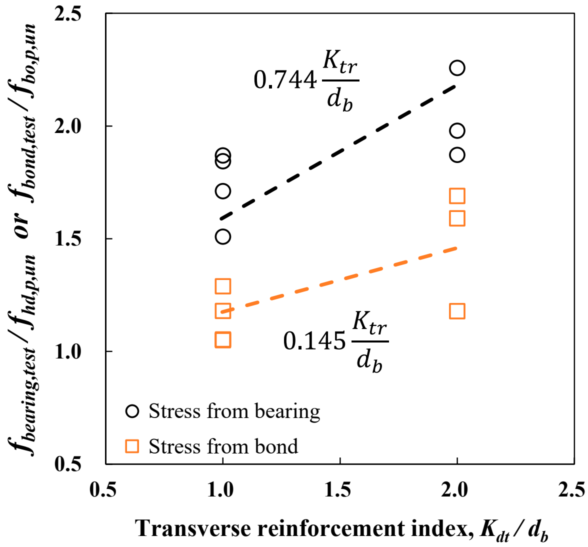

Figure 13. Correlation between transverse reinforcement index and stresses from head bearing or bond.

4.5. Proposal and Validation of an Anchorage Strength Model for Headed Bars

Based on the regression relationships derived in Sections 4.1–4.4, an empirical model is proposed to predict the anchorage strength of large-diameter headed bars anchored at the cutoff point. The proposed formulation decomposes the anchorage resistance into two components, as expressed in Equation (8): a head-bearing component ($f_{hd,p}$) at the enlarged head and a bond component ($f_{bo,p}$) along the deformed bar. The effects of the experimental variables were incorporated into each component in the form of confinement factors.

$$f_{dt,p} = f_{hb,p} + f_{bo,p} \quad (8)$$

To incorporate the effects of effective concrete thickness and transverse reinforcement, the coefficients defined in Equations (6) and (7) were applied to each component of Equation (8), which can be rearranged as Equations (9) and (10).

$$f_{hd,p} = 8.14\varphi_{hb}\sqrt{f'_c} \quad (9)$$

$$f_{bo,p} = 2.56\varphi_{bo}\frac{l_{dt}}{d_b}\sqrt{f'_c} \quad (10)$$

Accordingly, the predicted anchorage strength of a headed bar anchored at the cutoff point is proposed as expressed in Equation (11):

$$\begin{aligned} f_{dt,p} = {} & 8.14\left(0.484\tfrac{c_{min}}{d_b} + 0.744\tfrac{K_{tr}}{d_b} + 0.473\right)\sqrt{f'_c} \\ & + 2.56\left(0.224\tfrac{c_{min}}{d_b} + 0.145\tfrac{K_{tr}}{d_b} + 0.594\right)\tfrac{l_{dt}}{d_b}\sqrt{f'_c} \end{aligned} \quad (11)$$

To prevent extrapolation beyond the experimental range and to avoid unconservative predictions, the following limits were imposed:

- Predicted anchorage strength: $f_{dt,p} \leq 587$ MPa;
- Concrete compressive strength: $f_c' \leq 75.8$ MPa;
- Diameter of bar: 43 mm $\leq d_b \leq$ 57 mm;
- Net bearing area of the head: $A_{brg} \geq 4.0\ A_b$ (only circular heads type);

- Development length: $l_{dt} \leq 28\ d_b$;
- Effective concrete thickness: $c_{min} \geq 1.0d_b$;
- Transverse reinforcement: $K_{tr} \leq 2.0d_b$ (only closed stirrups type).

These limitations directly correspond to the parameter ranges used in the regression analyses and are essential for consistent application of the proposed model to cutoff point anchorage conditions. To address potential concerns regarding coefficient sign instability arising from the limited sample size, the statistical significance and confidence intervals of the estimated regression coefficients were systematically examined. All regression coefficients remained statistically significant at the 95% confidence level, and their corresponding confidence intervals did not include zero. Moreover, the estimated coefficients consistently exhibited the expected directional influence, thereby supporting the robustness of the model formulation within the investigated parameter range. To validate the proposed anchorage strength model for headed bars anchored at the cutoff point, as expressed in Equation (11), the experimental results of 12 unconfined specimens and 7 confined specimens from this study were compared with the predicted values. As shown in Figure 14a, the mean test-to-prediction ratio was 0.99, indicating a very close agreement between the experimental and predicted results. The coefficient of variation (COV) was 4.72%, demonstrating very low scatter in the prediction accuracy.

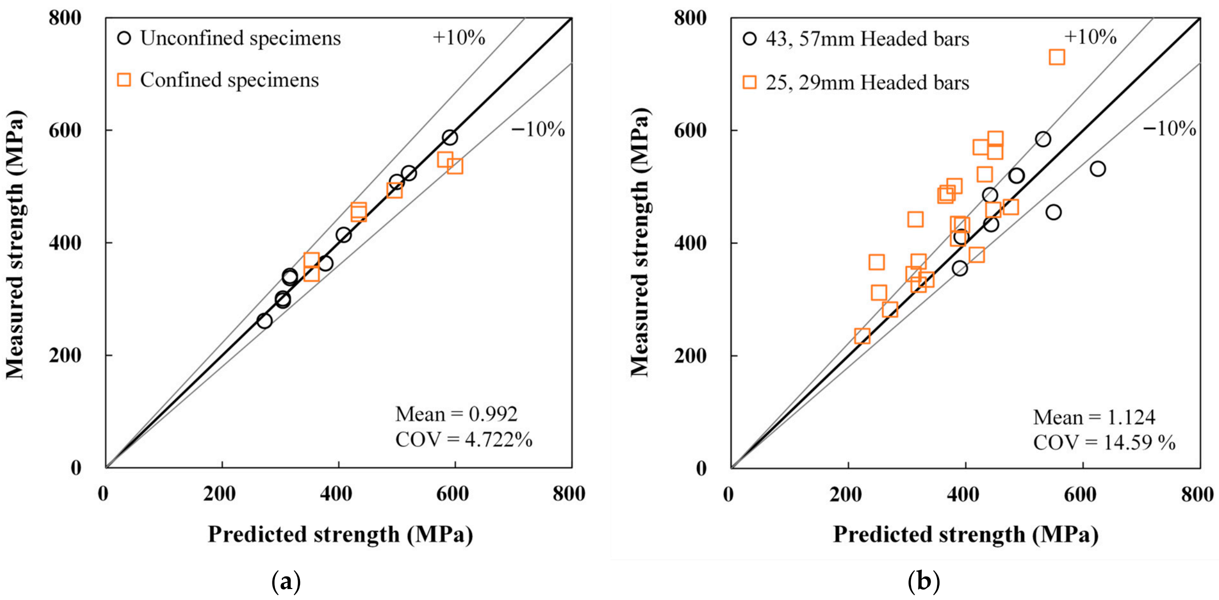

Figure 14. Validation of an anchorage strength model: (**a**) present test specimens; (**b**) previously reported test specimens.

The proposed anchorage strength model was further evaluated using independent experimental results from previous studies. Since no prior tests were conducted on headed bars anchored at the cutoff point, lap-splice test results exhibiting similar failure behavior were adopted for comparison. Although the two configurations differ in load path and boundary conditions, their equivalence is defined at the level of the governing mechanism. In both test configurations, anchorage resistance is governed by splitting-controlled failure of the surrounding concrete induced by bond stresses, head-bearing wedging forces, and prying action associated with flexural deformation. Therefore, the validation is interpreted within this mechanism-based comparability domain, and the proposed model should be applied within this defined boundary. Because cutoff anchorage generally involves steeper stress gradients and more localized stress concentrations than lap-splice conditions, validation using lap-splice data may result in mildly conservative predictions within the examined parameter ranges.

The comparison dataset comprised 23 specimens with 25- and 29-mm headed bars [24] and 9 specimens with 43- and 57-mm headed bars [29], totaling 32 specimens. As shown in Figure 14b, the overall mean test-to-prediction ratio for the 32 specimens was 1.12. For the 25- and 29-mm headed bars, the mean ratio was 1.18, whereas for the 43- and 57-mm headed bars, the mean ratio was 0.99. The comparison indicates that the proposed model tended to predict higher anchorage strengths for smaller-diameter headed bars relative to larger-diameter bars. This size-dependent behavior can be consistently interpreted within the geometric scaling framework outlined in the Introduction. With increasing bar diameter, the tensile force demand scales with the bar cross-sectional area, whereas the interfacial area available for anchorage stress transfer increases only proportionally to the perimeter, thereby necessitating higher average anchorage stresses for larger-diameter bars. Furthermore, the diameter-dependent amplification of rib-induced radial pressure intensifies the circumferential tensile stresses in the surrounding concrete, which in turn accelerates the initiation and propagation of splitting cracks. This trend is consistent with previous research findings reporting that the anchorage strength generally decreases with increasing bar diameter [9–13,16,17,30]. These results suggest that the influence of bar diameter on anchorage performance should be carefully considered when estimating the development length for large-diameter headed bars. Therefore, additional research focusing on the effect of bar diameter on anchorage behavior is warranted.

5. Conclusions

The anchorage behavior and strength of large-diameter headed bars (43 and 57 mm) anchored at cutoff points were experimentally evaluated, and a regression-based predictive model was proposed. Nineteen RC beam specimens were tested under four-point loading. The main variables were the development length, clear side cover, clear spacing between headed bars, transverse reinforcement index, and concrete compressive strength.

All the specimens exhibited splitting-controlled failure characterized by longitudinal cracking along the development region and cover spalling near the head. The anchorage mechanism was governed by the combined action of wedging forces induced by head bearing, bond stresses developed along the development length, and prying action associated with flexural deformation. In the unconfined condition without transverse reinforcement, crack localization and cover spalling progressed rapidly, resulting in a pronounced brittle degradation of load-carrying capacity. In contrast, under confined conditions with transverse reinforcement, the transverse reinforcement effectively restrained crack propagation, leading to a more distributed cracking pattern and an improvement in deformation capacity relative to the unconfined specimens.

The anchorage strength increased with increasing concrete compressive strength and development length. A reduction in effective concrete thickness, governed by side cover and bar spacing, resulted in a corresponding decrease in anchorage strength. Among the parameters investigated, transverse reinforcement was identified as the most influential variable, and its confinement effect resulted in a substantial enhancement of the anchorage strength. On average, the confined specimens exhibited approximately 39.8% higher anchorage strength than the unconfined specimens.

From the perspective of the stress transfer mechanism, the anchorage strength can be interpreted as the sum of the head-bearing component and the bond component. At the ultimate state, the bond component was estimated to account for approximately 70–86% of the total developed stress, whereas the head-bearing component contributed about 14–30%. With increasing effective concrete thickness, both the bond and head-bearing stresses increased. Transverse reinforcement restrained the growth of splitting cracks and the prying action, thereby enhancing the anchorage performance and promoting the development of the head-bearing component.

Based on the experimental observations and regression analyses, an anchorage strength model incorporating variable into separate bond and head-bearing components was proposed. The proposed model showed a very good agreement with the present test results, yielding a mean test-to-prediction ratio of 0.99 and a coefficient of variation of 4.72%. Additional validation using headed-bar lap-splice test data reported in the literature indicated that the proposed model provides reasonably accurate predictions for large-diameter bars of the same size; however, it was found to systematically predict higher anchorage strengths for bars with smaller diameters.

The present findings provide preliminary evidence and a technical basis for potential future development or refinement of design provisions related to large-diameter headed bars. It should also be noted that the proposed anchorage strength formulation is applicable to splitting-controlled conditions with prying action observed in the present experimental program and is valid within the investigated geometric and material parameter ranges. Application beyond these ranges or to other failure mechanisms requires additional verification. These results also suggest that current design limitations could potentially be expanded to accommodate larger bar diameters. The significant influences of transverse reinforcement and effective concrete thickness indicate that these parameters may need to be more explicitly considered in anchorage design provisions. Moreover, further refinement of the proposed formulation into a simplified and implementation-oriented format would facilitate its integration into code-based design procedures and practical engineering applications.

However, broader validation across a wider range of geometric configurations and material properties would be required before such findings could support formal revisions to existing design codes. To further extend and generalize the applicability of the proposed model, future research should examine intermediate bar diameters (e.g., 29 mm and 36 mm) to clarify potential size-dependent effects. Systematic evaluation of side cover and spacing parameters, headed bar geometry, and alternative transverse reinforcement configurations is also recommended to better understand their influence on splitting resistance, bearing stress distribution, and confinement efficiency. Such investigations would improve the general applicability of the proposed model.

Funding: This research was funded by National Research Foundation of Korea (NRF-2021R1C1C1014263).

Institutional Review Board Statement: Not applicable.

Informed Consent Statement: Not applicable.

Data Availability Statement: The original contributions presented in this study are included in the article.

Conflicts of Interest: The author declares no conflicts of interest.

References

1. Eligehausen, R.; Mallée, R.; Silva, J.F. *Anchorage in Concrete Construction*; John Wiley & Sons: New York, NY, USA, 2012.
2. Darwin, D.; Dolan, C.W.; Nilson, A.H. *Design of Concrete Structures*, 16th ed.; McGraw-Hill: New York, NY, USA, 2021.
3. Bashandy, T.R. Application of Headed Bars in Concrete Members. Ph.D. Thesis, University of Texas at Austin, Austin, TX, USA, 1996.
4. Wright, J.L.; McCabe, S.L. *The Development Length and Anchorage Behavior of Headed Reinforcing Bars*; SM Report No. 44; University of Kansas Center for Research: Lawrence, KS, USA, 1997.

5. Thompson, M.K.; Ledesma, A.; Jirsa, J.O.; Breen, J.E. Lap splices anchored by headed bars. *ACI Struct. J.* **2006**, *103*, 271–279. [CrossRef] [PubMed]
6. ACI Committee 318. *Building Code Requirements for Structural Concrete (ACI 318-19) and Commentary (ACI 318R-19)*; American Concrete Institute: Farmington Hills, MI, USA, 2019.
7. *KDS 14 20 52*; Korea Design Standard. Korea Construction Standards Center: Seoul, Republic of Korea, 2021.
8. Chun, S.-C.; Choi, C.-S.; Jung, H.-S. Side-face blowout failure of large-diameter high-strength headed bars in beam–column joints. *ACI Struct. J.* **2017**, *114*, 161–172. [CrossRef]
9. Ghimire, K.; Darwin, D.; O'Reilly, M. *Anchorage of Headed Reinforcing Bars in Concrete*; SM Report No. 127; University of Kansas Center for Research: Lawrence, KS, USA, 2018.
10. Banaeipour, A. Development of Large High-Strength Reinforcing Bars with Standard Hooks and Heads. Ph.D. Thesis, University of Kansas, Lawrence, KS, USA, 2023.
11. Nazzal, L.A.; Darwin, D.; O'Reilly, M. *Anchorage of High-Strength Reinforcing Bars in Concrete*; SM Report No. 150; University of Kansas Center for Research: Lawrence, KS, USA, 2023.
12. Shao, Y.; Darwin, D.; O'Reilly, M.; Lequesne, R.D.; Ghimire, K.; Hano, M. *Anchorage of Conventional and High-Strength Headed Reinforcing Bars*; SM Report No. 117; University of Kansas Center for Research: Lawrence, KS, USA, 2016.
13. Sim, H.-J.; Chun, S.-C.; Kim, I.-H. Side-face blowout strength of large-diameter high-strength headed bars in a single layer or two layers terminated within exterior beam-column joints. *J. Struct. Eng.* **2023**, *149*, 04022233. [CrossRef]
14. Biscaia, H.C. Experimental and numerical evaluations of the bond behaviour between ribbed steel rebars and concrete. *Arch. Civ. Mech. Eng.* **2023**, *23*, 159. [CrossRef]
15. Liang, Z.; Gong, C.; Liang, W.; Zhang, S.; Li, X. Behavior of confined headed bar connection for precast reinforced concrete member assembly. *Appl. Sci.* **2023**, *13*, 827. [CrossRef]
16. Hung, C.-C.; Yuen, T.Y.P.; Huang, C.-W.; Yen, C.-H. Tension lap splices in UHPC beams: Influence of rebar size, steel fibers, splice length, and coarse aggregate. *J. Build. Eng.* **2022**, *55*, 104716. [CrossRef]
17. Huang, Y.; Yu, Z. Experimental study of the bonding behavior between coarse aggregate ultra-high performance concrete and steel rebar. *Eng. Struct.* **2023**, *288*, 116253. [CrossRef]
18. Xie, Y.; Xiong, E.; Gong, Z.; Zhang, J.; Gao, Y.; Taciroglu, E. Experimental study on bond performance of staggered lap rebars in ultra-high performance concrete (UHPC). *Constr. Build. Mater.* **2024**, *433*, 136756. [CrossRef]
19. Hu, X.; Xue, W.; Lv, Y. Bond properties between lapped steel rebars and UHPC under direct tension. *Constr. Build. Mater.* **2023**, *408*, 133761. [CrossRef]
20. Lagier, F.; Massicotte, B.; Charron, J.-P. Bond strength of tension lap splice specimens in UHPFRC. *Constr. Build. Mater.* **2015**, *93*, 937–949. [CrossRef]
21. Thompson, M.K. The Anchorage Behavior of Headed Reinforcement in CCT Nodes and Lap Splices. Ph.D. Thesis, University of Texas at Austin, Austin, TX, USA, 2002.
22. Thompson, M.K.; Jirsa, J.O.; Breen, J.E. Behavior and capacity of headed reinforcement. *ACI Struct. J.* **2006**, *103*, 522–530. [CrossRef] [PubMed]
23. Thompson, M.K.; Jirsa, J.O.; Ledesma, A.L.; Breen, J.E.; Klinger, R.E. *Anchorage Behaviour of Headed Reinforcement*; Report No. 1855-3; Center for Transportation Research, University of Texas at Austin: Austin, TX, USA, 2002.
24. Chun, S.-C. Lap splice tests using high-strength headed bars of 550 MPa (80 ksi) yield strength. *ACI Struct. J.* **2015**, *112*, 679–688. [CrossRef]
25. Sim, H.-J.; Chun, S.-C. Side-face blowout failure of headed bars in high-strength concrete. *ACI Struct. J.* **2022**, *119*, 221–231.
26. Chun, S.-C.; Lee, B.-S. Components of side-face blowout strengths of headed bars in exterior beam-column joints. *ACI Struct. J.* **2019**, *116*, 159–170.
27. Kao, A.M. Tensile Steel Requirements at Inflection and Bar Cutoff Points in Reinforced Concrete Beams. Ph.D. Thesis, Iowa State University, Ames, IA, USA, 1969.
28. Ferguson, P.M.; Husain, S.I. *Strength Effect of Cutting off Tension Bars in Concrete Beams*; Center for Highway Research, University of Texas at Austin: Austin, TX, USA, 1967.
29. Lee, S.Y. Strength of Lap Splices Anchored by Large Diameter Headed Bars. Master's Thesis, Mokpo National University, Mokpo, Republic of Korea, 2014; pp. 67–68.
30. Blessent, M.; Darwin, D.; Lepage, A.; Lequesne, R.D.; O'Reilly, M. *Anchorage of Large High-Strength Reinforcing Bars with Standard Hooks and Heads: Initial Tests*; SL Report 20-3; University of Kansas Center for Research: Lawrence, KS, USA, 2020.
31. *ASTM C39/C39M-24*; Standard Test Method for Compressive Strength of Cylindrical Concrete Specimens. ASTM International: West Conshohocken, PA, USA, 2024.
32. Collins, M.P.; Mitchell, D. *Prestressed Concrete Structures*; Prentice Hall: Upper Saddle River, NJ, USA, 1991.

33. Orangun, C.O.; Jirsa, J.O.; Breen, J.E. A reevaluation of test data on development length and splices. *ACI J. Proc.* **1977**, *74*, 114–122.
34. ACI Committee 408. *Bond and Development of Straight Reinforcing Bars in Tension (ACI 408R-03)*; American Concrete Institute: Farmington Hills, MI, USA, 2003.

Disclaimer/Publisher's Note: The statements, opinions and data contained in all publications are solely those of the individual author(s) and contributor(s) and not of MDPI and/or the editor(s). MDPI and/or the editor(s) disclaim responsibility for any injury to people or property resulting from any ideas, methods, instructions or products referred to in the content.

https://doi.org/10.3390/app16052599